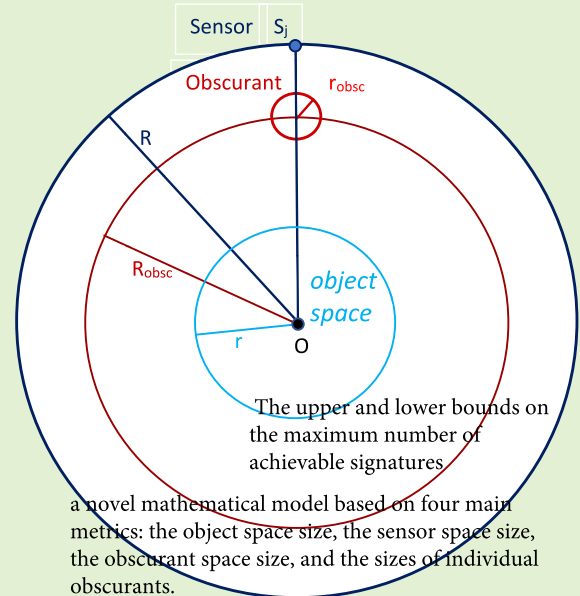


Optimal Design for Modulated Binary Sensors

Alina Olteanu^{1b}, Member, IEEE, Longxiang Luo^{2b}, Member, IEEE, Yang Xiao^{3b}, Fellow, IEEE, and Wei Liang^{4b}, Senior Member, IEEE

Abstract—A paramount factor limiting the applications of binary sensors is these sensors' on-off property outputting binary digits of "0" or "1". To overcome this limitation, modulators or obscurants are added to enhance the sensing ability of binary sensors and render them usable in applications such as multi-target tracking and human activity recognition. Obscurants segment the field of interest into subregions and distinguish each subregion by a list of sensor states called signatures. This paper studies two placement scenarios in a two-dimensional planar graph. In the first scenario, we prove upper and lower bounds on the maximum number of achievable signatures. In the second scenario, starting from the placement of sensors and obscurants in which the maximum number of signatures is achievable, we propose a novel mathematical model based on four main metrics: the object space size, the sensor space size, the obscurant space size, and the sizes of individual obscurants. We find the minimum and maximum radiuses that bound the object detection area given the number and sizes of sensors and obscurants. We derive the obscurant space size as a function of the object space size and the size of individual obscurants. We also provide a linear relationship formula between the obscurant space radius, the sensor space radius, and the obscurants' radiuses and conduct modeling experiments to study the relationship between these metrics. Finally, we deduct an explicit formula for the maximum obscurant space size for the sensor space and the individual obscurant sizes.

Index Terms—Binary sensors, sensor array, reference structure, sensor deployment, optimization, modulator, obscurant, signature, theoretical analysis.



Manuscript received 16 May 2022; accepted 16 July 2022. Date of publication 29 July 2022; date of current version 1 September 2022. The work of Longxiang Luo and Wei Liang was supported in part by National Key Research and Development Program under Grant 2021YFB3301001, in part by the Liaoning Revitalization Talents Program under Grant XLYC1902110, and in part by the National Natural Science Foundation of China under Grant 62022088. The associate editor coordinating the review of this article and approving it for publication was Dr. Prosanta Gope. (Corresponding authors: Yang Xiao; Wei Liang.)

Alina Olteanu is with the Department of Biology, Chemistry, Mathematics and Computer Science, University of Montevallo, Montevallo, AL 35115 USA (e-mail: aolteanu@montevallo.edu).

Longxiang Luo is with the State Key Laboratory of Robotics, Shenyang Institute of Automation, Chinese Academy of Sciences, Shenyang 110016, China, also with the Key Laboratory of Networked Control Systems, Chinese Academy of Sciences, Shenyang 110016, China, also with the Institutes for Robotics and Intelligent Manufacturing, Chinese Academy of Sciences, Shenyang 110016, China, and also with the University of Chinese Academy of Sciences, Beijing 100190, China (e-mail: robbieluo@yeah.net).

Yang Xiao is with the Department of Computer Science, The University of Alabama, Tuscaloosa, AL 35487 USA (e-mail: yangxiao@ieee.org).

Wei Liang is with the Shenyang Institute of Automation, Chinese Academy of Sciences, Shenyang 110016, China, also with the State Key Laboratory of Robotics, Shenyang Institute of Automation, Chinese Academy of Sciences, Shenyang 110016, China, also with the Key Laboratory of Networked Control System, Shenyang Institute of Automation, Chinese Academy of Sciences, Shenyang 110016, China, and also with the Institutes for Robotics and Intelligent Manufacturing, Chinese Academy of Sciences, Shenyang 110169, China (e-mail: weiliang@sia.cn).

Digital Object Identifier 10.1109/JSEN.2022.3193628

I. INTRODUCTION

SENSORS and sensor networks have many applications in various fields [1]. Furthermore, arrays of sensors are also very popular in both practical and theoretical studies. Reference structures, also known as modulators or obscurants, are materials distributed in the radiation space between an object and a measurement system to modulate radiation properties such as absorption, permittivity, and polarization [2]. Reference structures are mostly applied in object analysis, including imaging, where object analysis encompasses parameter estimation, and classification [2], [3]. For parameter estimation, including location, orientation, velocity, or trajectory, there are many applications such as target counting [4]–[7], localization [8], [9] and multi-target tracking [10]–[13]. For classification, as in object identity, type, or group, current applications focus mainly on human activity recognition [14]–[19]. In such applications, reference structures enhance the spatial awareness of binary sensors. Binary sensors with reference structures exhibit enhanced spatial awareness and can locate and track intrusion more accurately. Since video cameras are widely used, binary sensor networks equipped with reference structures appear redundant. However, the combination of reference structure and binary sensor

networks is attracting increased investigation due to enhanced privacy protection and good performance in low-cost, low power consumption networks.

Reference structure is founded in computational imaging theory [2], [20]–[24]. The authors in [20] give the continuous and discrete geometric models of the measurement equation with reference structure by quantifying the one-dimension light pipes connecting target and sensor elements with binary bits and constructing the transformation matrix based on the Hadamard matrix. With three-dimensional plastic beads modulating sensor sense views, the authors in [21] study the reconstruction of source-target on a three-dimensional plane from measurements on a two-dimensional focal plane. A sensor array system is applied to accurately estimate the size of a two-dimensional object without ever forming a physical image [22]. Based on reference structures, a motion tracking system is implemented to detect human motion in one of 15 cells in a $1.6m \times 1.6m$ area [24]. The authors in [2] introduce a compressive measurement system to tomography imaging with reference structure. Utilizing reference structure tomography and binary sensors to segment the field of interest (FOI) into cells, the researchers give the upper and lower bounds of distinct signatures that can be realized in deployment models [24].

Based on the theoretical foundations of David J. Brady in [2], [24], researchers promote the study of reference structure in three main aspects: design shapes of reference structure, segmentation of the FOI, and coding the segmented subregions (or cells) of the FOI. The shapes of reference structures encompass fence form [11], fan shape [16], ring shape [16], lotus form [17], hemisphere-shape [25], [26], cylinder shell-shape [26], hollow-carved disk [27] etc. For the segmentation of the FOI, the authors in [30] provide an upper bound on the number of unique cells which have common edges with the boundary of the FOI. In [31], a tool is provided to acquire the segmentation information of the FOI, such as the number of subregions and their codes. The necessary and sufficient conditions to segment the FOI into the maximum number of cells are presented in [32]. The authors in [33], [34] prove that the maximum number of signatures with a certain number of sensors can be achieved using an unlimited number of obscurants to modulate the sensors' views.

In this paper, we first study an initial placement scenario of sensors and modulators and determine upper and lower bounds on the maximum number of signatures achieved. We then extend our sensor-modulator placement model based on the design in [34]. We use this deployment model as a starting point since the maximum number of signatures is achievable in this scenario ([34]). While [34] studies maximizing the number of signatures, in this paper, we focus on the influence of reference structure on binary sensor deployments in a placement scenario in which the maximum number of signatures is achievable. More specifically, we build a novel mathematical model for sensors and obscurants, taking into account four main metrics: the object space size, the sensor space size, the obscurant space size, and the sizes of individual obscurants as well as the relationships between them. The contributions of

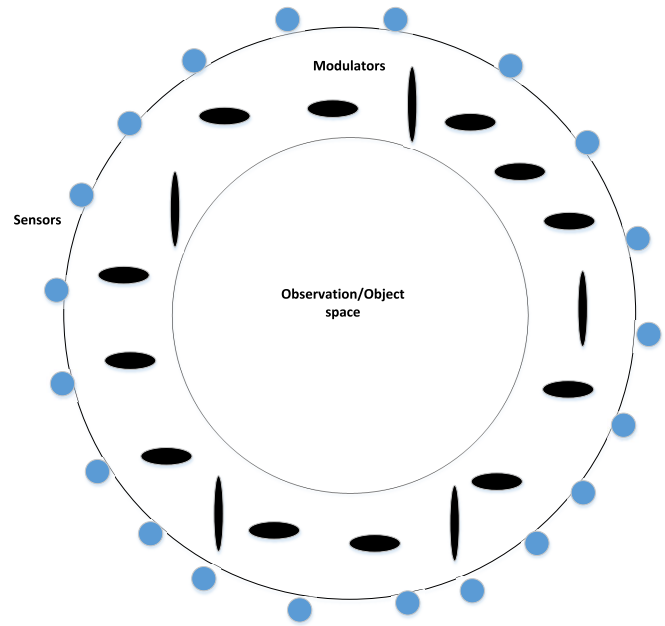


Fig. 1. A sensor array with an observation space.

this paper in the second deployment scenario are summarized as follows:

- We determine explicit analytic formulas for the minimum and maximum object space size relative to the size of the sensor space, the obscurant space, and the sizes of the individual obscurants.
- We provide a formula for the obscurant space size as a function of the object space and the size of individual obscurants.
- We deduce a linear relationship formula and conduct experiments to study the relationships among the following metrics: the sensor space radius, the radius of an obscurant, and the radius of the circle on which the centers of all obscurants are located.
- Finally, we derive an explicit expression for the maximum obscurant space size in terms of the sensors' space and the individual obscurant sizes.

The rest of the paper is organized as follows. Section II introduces the initial research model and proves upper and lower bounds on the maximum number of signatures in this scenario. Section III describes our detailed mathematical model and main analytical results. Section IV presents experimental results related to four metrics: object space radius, sensor space radius, obscurant space radius, and each obscurant's radius. We conclude the paper in Section V.

II. INITIAL MODEL AND THEORETIC STUDIES

We start with the study of a modulated sensor system deployment in a two-dimensional planar graph as in Fig. 1.

Based on Fig. 1 and the assumptions in [29], [31], we give the following definitions:

- The object space where target objects can be detected is shaped as a disk and denoted as Σ .

- The detection space, denoted as X , is also shaped as a disk (see Fig. 1).
- Modulators/obscurants are deployed in the region between the detection line (border of the detection space) and the object space (see Fig. 1).
- Sensors are deployed on the detection line, and obscurants (reference structures) are deployed between sensors and target objects. For m sensors and n obscurants, we have $S = s_0, \dots, s_{m-1}$ and $O = o_0, \dots, o_{n-1}$.
- For any location $p \in \Sigma$ and $s_i \in S$, if p is visible to sensor s_i , we have $\chi_i(p) = 1$. Otherwise, p is not visible to sensor s_i and $\chi_i(p) = 0$. For all the m sensors, let $\chi : \Sigma \rightarrow \{0, 1\}^m$ and $\chi(p) = \chi_{m-1}(p) \dots \chi_0(p)$, where $\chi(p)$ is the signature of location p .
- The distinct signatures corresponding to locations in the object space are denoted as $\Pi(S, O, \Sigma) = \{\chi(p) | p \in \Sigma\}$. By setting $\pi(S, O, \Sigma) = |\Pi(S, O, \Sigma)|$, we define $\pi(m, n) = \max_{|S|=m, |O|=n} \pi(S, O, \Sigma)$, the maximum number of distinct signatures realized by a system with m sensors and n obscurants.

Given the scenario described above, we present upper and lower bounds on the maximum number of signatures when the object space is large. The first two theorems focus on the case where obscurants are placed along a circle between the detection line and the object space, while theorems and study the case where obscurants are placed along with several concentric circles between the detection line and the object space.

Theorem 1: In a sensor system, shown in Fig. 1, m point sensors are placed along a circle (detection line) at equal intervals. The object space is a disk. n obscurants are placed along a circle between the detection circle and object space. Under the assumption that at least 2 sensors cover each point and that the radius of the object space is large enough, the curves along which both the sensors and obscurants are placed can be approximated by parallel lines. In this case, an upper bound of $\pi(m, n)$ is $O(m^2 n^2)$.

Proof: Each sensor is associated with one obscurant, therefore assuming 2 sensors and 2 obscurants, this leads to 4 signatures: 00, 01, 10 and 11. Generalizing, we can form

$$\binom{m}{2} = m(m-1)/2$$

different groups of 2 sensors out of the total of m sensors. Similarly, we can form $\binom{n}{2}$ different groups of 2 obscurants out of the total of n obscurants. Therefore any 2 sensors coupled with any 2 obscurants will create at most 4 signatures. This yields:

$$\begin{aligned} \pi(m, n) &= 4 \binom{m}{2} \binom{n}{2} = m(m-1)n(n-1) < m^2 n^2 \\ \Rightarrow \pi(m, n) &= O(m^2 n^2). \end{aligned}$$

Theorem 2: In a sensor system, shown in Fig. 1, m point sensors are placed along a circle (detection line) at equal intervals. The object space is a disk. n obscurants are placed along a circle which is between the detection space and the

object space. Under the assumption that the radius of the object space is large enough, the curves along which both the sensors and obscurants are placed can be approximated by parallel lines. Since we are studying a large object space, we assume a sensor system with at least 3 sensors and modulators, i.e. $m, n \geq 3$. In this case, for each L such that $\frac{1}{2}(e+1) < L < \frac{m}{\log(m)}$, a lower bound of $\pi(m, n)$ is $\Omega\left(\frac{8\log(3)}{3} \frac{L \log(L)mn}{\log[L \log(L)mn]}\right)$. Here we denote $\log(x) := \log_e(x) = \ln(x)$, $x > 0$.

Proof: Function $f(x) = x \log(x)$ is strictly convex on interval $(0, \infty)$, since $f''(x) = (\log(x) + 1)' = 1/x > 0$, $\forall x > 0$. Consider the following property of convex differentiable functions on $(0, \infty)$:

$$f(x) \geq f(x_0) + f'(x_0)(x - x_0), x_0, x \in (0, \infty) \quad (1)$$

The geometric interpretation of inequality (1) is that the graph of a convex, differentiable function is above the tangent drawn through any point $(x_0, f(x_0))$ to the graph. By replacing $f(x) = x \log(x)$, $x = L$, $x_0 = e$ in (1) we have:

$$\begin{aligned} L \log(L) &\geq e + (\log(e) + 1)(L - e) = e + 2(L - e) \\ &= 2L - e > 1 \end{aligned} \quad (2)$$

The last inequality in (2) is equivalent with the hypothesis $\frac{1}{2}(e+1) < L$. Therefore:

$$\begin{aligned} 1/\log[L \log(L)mn] &= 1/(\log(L \log(L)) + \log(mn)) \\ &\leq 1/(\log(2L - e) + \log(mn)) \\ &< 1/\log(mn) \end{aligned}$$

By also using the assumption $L < m/\log(m)$, we have

$$\begin{aligned} \frac{L \log(L)mn}{\log[L \log(L)mn]} \\ \pi(m, n) &< \frac{\frac{m}{\log(m)} \log\left(\frac{m}{\log(m)}\right)mn}{\log(mn)m(m-1)n(n-1)} \\ &= \frac{m-1+1}{m-1} \frac{1}{n-1} \frac{1}{\log(mn)} \frac{\log(m) - \log(\log(m))}{\log(m)} \\ &< \left(1 + \frac{1}{2}\right) \frac{1}{2} \frac{1}{\log(3^2)} = \frac{3}{8 \log(3)} \\ \Rightarrow \pi(m, n) &> \frac{8 \log(3)}{3} \frac{L \log(L)mn}{\log[L \log(L)mn]} \end{aligned}$$

Theorem 3: In a sensor system, shown in Fig. 1, m point sensors are placed along a circle (detection line) at equal intervals. The object space is a disk. n obscurants are placed along with several circles between the detection space and the object space. Under the assumption that the radius of the object space is large enough, the curves along which both the sensors and obscurants are placed can be approximated as several parallel lines. In this case, an upper bound of $\pi(m, n)$ is $O(m^2 n^2)$.

Proof: This is a consequence of Theorem 1. Let there be a pair of sensors and a pair of obscurants, such that they generate at most 4 different signatures. Consider a new pair of obscurants on the same horizontal as the first pair. Together with the first pair, this new pair generates at most 4 signatures. Therefore, given 2 sensors and 4 obscurants,

there are $4 + 4 = 8$ different signatures. If however, each of the 2 pairs of obscurants are placed on distinct parallel lines, then, given 2 sensors and 4 obscurants, there are only 4 different signatures. Therefore we may have less signatures than in Theorem 1. It implies:

$$\begin{aligned} \pi(m, n) &\leq \pi_{\text{Theorem 1}}(m, n) < m^2 n^2 \\ &\Rightarrow \pi(m, n) = O(m^2 n^2) \end{aligned}$$

One can give examples of a pair of sensors and a pair of obscurants for which the signature 00 does not appear. ■

Theorem 4: In a sensor system, shown in Fig. 1, m point sensors are placed along a circle (detection line) at equal intervals. The object space is a disk. n obscurants are placed along k circles which are all between the detection space and the object space. Under the assumption that the radius of the object space is large enough, the curves along which both the sensors and obscurants are placed can be approximated as k parallel lines, with n/k obscurants on each line and $n/k \geq 3$. We assume n/k to be an integer and $m, n \geq 3$. In this case, a lower bound of $\pi(m, n)$ is $\Omega\left(\frac{L \log(L)mn}{\log[L \log(L)mn/k]}\right)$, where $\frac{1}{2}(e+1) < L < \frac{m}{\log(m)}$.

Proof: According to Theorem 2, for $n/k \geq 3$ on a line we have:

$$\pi(m, n/k) \geq \frac{8}{3} \log(3) \frac{L \log(L)mn/k}{\log[L \log(L)mn/k]}$$

Given that we have k horizontal lines, we obtain:

$$\pi(m, n) = k\pi(m, n/k) \geq \frac{8}{3} \log(3) \frac{L \log(L)mn}{\log[L \log(L)mn/k]}$$

III. DETAILED MODEL AND THEORETIC STUDIES

In this section, we extend the placement model from Section II with a set of concrete assumptions, starting from the study of a modulated sensor system that achieves the maximum number of signatures ([34]). In this model shown in Fig. 2, sensors and obscurants are deployed in a two-dimensional planar graph under the following assumptions: a sensor is a point, an obscurant is a disk, the sensor space, and the object space are both disks of different radiuses. Sensors are deployed at equal intervals from one another. Similarly, obscurants are deployed at equal intervals from one another. The obscurants are placed between the detection line and the object space on a circle.

We consider the case when $m = n$, i.e., each sensor corresponds to an obscurant. In Fig. 2, let R be the radius of the sensor space X , and r be the radius of the object space, Σ , with $R > r$.

For the sake of simplicity, we assume that all obscurants are disk-shaped, of the same radius r_{obsc} . These conditions are not too restrictive. Indeed, if an obscurant is not disk-shaped, we replace it with the disk of minimum radius, which contains the obscurant. We then choose the largest of these radiuses. Each obscurant will be contained in the disk corresponding to the maximum radius. Each sensor corresponds to an obscurant, such that the center of the disk of an obscurant o_j , the sensor

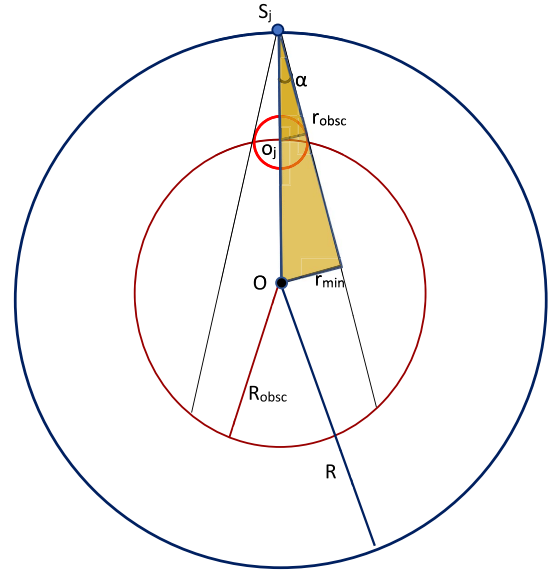


Fig. 2. A sensor system.

S_j corresponding to obscurant o_j and the center O of the detection space are three collinear points, $j = 0, 1, \dots, m-1$. Assume also that the centers of all obscurants are situated on a circle centered at O of radius R_{obsc} such that $R_{\text{obsc}} + r_{\text{obsc}} < R$. (see Fig. 2).

The maximum number of signatures, 2^n , as proven in [34], is achievable under the assumptions above.

We are interested in the case when r , the radius of the object space, is large. Conversely, suppose r is small enough relative to the radius of each obscurant r_{obsc} . In that case, the object space will be completely contained in the shadow created by the obscurant, and the corresponding sensor will detect no object to the obscurant. Repeating the same process for all sensor-obscurant pairs, the object space will not be visible to any of the sensors, and therefore $\pi(m, n) = 1$ with the only signature being $00 \dots 0$.

Following, we determine the minimum and maximum radiuses for the object space relative to the size of the sensor space and the size of each obscurant. We also provide a way to fine-tune the sensor-obscurant pair angle based on the obscurant's size, the sensor space size, and the size of the obscurant space.

Theorem 5: In a sensor system, shown in Fig. 2, m point sensors are placed along a circle (detection line) at equal intervals. The detection circle has given radius R . The object space is shaped like a disk of radius r . m obscurants are placed along a circle between the detection circle and the object space. The number of obscurants is the same as the number of sensors, as each obscurant is associated with a sensor. We assume $R > 6r_{\text{obsc}}$, that is, the radius of the sensor's space is at least six times larger than an obscurant's radius. This assumption is motivated by geometric and computational reasons (see Fig. 2 and proof below). We also assume $R - R_{\text{obsc}} = \lambda r_{\text{obsc}}$, $\lambda > 1$. This condition emerges naturally because obscurants are "in front of" sensors, between the sensors and the object space.

Then,

$$r_{\text{min}} = \frac{R r_{\text{obsc}}}{R - R_{\text{obsc}}}$$

and

$$r_{max} = R_{obs} - r_{obs}$$

In addition,

$$R_{obs} \in \left(\frac{(r_{obs} + R) - \sqrt{d}}{2}, \frac{(r_{obs} + R) + \sqrt{d}}{2} \right)$$

where

$$d = R^2 - 6Rr_{obs} + r_{obs}^2$$

is a necessary and sufficient condition for $r_{min} < r_{max}$. In this case, we can then choose r between r_{min} and r_{max} .

We also provide a way to fine tune the sensor-obscurant pair angle α by showing that

$$\alpha = 2 \arcsin \frac{1}{\lambda} \in (0, 180^\circ)$$

Proof: Let S_j be a sensor on the detection circle centered in O . We denote by o_j the center of the disk area of its corresponding obscurant. Consider the tangents from S_j to the circle of its corresponding obscurant. The radius of the obscurant's disk, drawn from o_j to the point of tangency, is perpendicular to the tangent ([36]), forming the smaller triangle in Fig. 2, highlighted in yellow. Also consider the perpendicular from O to the same tangent (see Fig. 2). Any radius of the object space smaller than the length of this perpendicular segment will define an object area that is completely obscured from the sensor. We denote the length of this segment to be r_{min} . We are therefore looking for a radius $r > r_{min}$. In order to determine r_{min} , consider the two triangles highlighted on yellow in Fig. 2. These two triangles are similar as the two segments of lengths r_{min} and r_{obs} are parallel, and S , o , and O are collinear. Applying Thales' theorem for basic proportionality [35], we have:

$$\begin{aligned} \frac{r_{min}}{r_{obs}} &= \frac{R}{R - R_{obs}} \\ \Leftrightarrow r_{min} &= \frac{Rr_{obs}}{R - R_{obs}} \end{aligned} \quad (3)$$

Since the obscurants are assumed to be outside of, or at most tangent to the object space, we have:

$$r_{max} = R_{obs} - r_{obs} \quad (4)$$

On the other hand, based on the hypothesis,

$$\begin{aligned} R &= R_{obs} + \lambda r_{obs} \\ \Rightarrow R &> R_{obs} + r_{obs} \end{aligned} \quad (5)$$

In order to choose r between r_{min} and r_{max} we need:

$$r_{min} < r_{max} \quad (6)$$

From (3) and (4), inequality (6) is equivalent to:

$$\begin{aligned} \frac{Rr_{obs}}{R - R_{obs}} &< R_{obs} - r_{obs} \\ \Leftrightarrow Rr_{obs} &< (R_{obs} - r_{obs})(R - R_{obs}) \\ \Leftrightarrow R_{obs}^2 - (r_{obs} + R)R_{obs} + 2Rr_{obs} &< 0 \end{aligned} \quad (7)$$

We consider the polynomial function:

$$p(x) := x^2 - (r_{obs} + R)x + 2Rr_{obs}, x \in R \quad (8)$$

The associated equation:

$$p(x) = 0 \quad (9)$$

has discriminant:

$$\begin{aligned} d &= (r_{obs} + R)^2 - 8Rr_{obs} = R^2 - 6Rr_{obs} + r_{obs}^2 \\ &\geq R(R - 6r_{obs}) > 0 \end{aligned} \quad (10)$$

Inequality (10) is true based on the assumption $R > 6r_{obs}$ in which the obscurants' radiuses are at least six times smaller than the radius of the detection space. Since d is positive, equation (8) has two distinct real solutions:

$$x_1 = \frac{(r_{obs} + R) - \sqrt{d}}{2}, x_2 = \frac{(r_{obs} + R) + \sqrt{d}}{2} \quad (11)$$

(7) is equivalent to:

$$R_{obs} \in \left(\frac{(r_{obs} + R) - \sqrt{d}}{2}, \frac{(r_{obs} + R) + \sqrt{d}}{2} \right) \quad (12)$$

Therefore (6) is satisfied by choosing R_{obs} as above and choosing r as in (6) is equivalent to R_{obs} as in (12).

For proving the pair angle formula, from Fig 2 we have:

$$\begin{aligned} \sin\left(\frac{\alpha}{2}\right) &= \frac{r_{obs}}{R - R_{obs}} = \frac{1}{\lambda} \\ \Leftrightarrow \alpha &= 2 \arcsin\left(\frac{1}{\lambda}\right) \end{aligned}$$

As shown in [34], α should be outside of this set of values $180 - i * 360/n | i = 1, \dots, (n/2) - 1$ in order to avoid overlapping edge lights. Corollary 1 allows for a suitable choice for λ and provides a way to deploy sensor-obscurant pairs to avoid unwanted α values in the set above.

Corollary 1: Since $\lambda r_{obs} = R - R_{obs} < R$ and R is given, finite, implies r_{obs} goes to zero when λ goes to infinity. Therefore we have shown that α takes all values in $(0, 180^\circ)$ when $\lambda \in (1, \infty)$.

The next theorem provides valuable insight into how to place obscurants relative to sensors and the center of the detection area, O (Fig. 2). We provide a formula for the obscurants' distance from the center of the detection area, O . We also derive the relationship between obscurants and sensors in terms of their distance from O .

Theorem 6: Let r be the radius of the object space, R the radius of the detection area, r_{obs} the radius of an obscurant, and R_{obs} the radius of the circle on which the centers of all obscurants are located. We will use the following notations:

$$R_{obs} = \beta r_{obs}, \text{ where } \beta = k\lambda \quad (13)$$

$$R - R_{obs} = \lambda r_{obs}, \text{ where } \lambda > 1, k > 1. \quad (14)$$

Then we obtain:

$$r_{min} = (k + 1)r_{obs} \quad (15)$$

$$k = \frac{R_{obs}}{R - R_{obs}} \quad (16)$$

and

$$q \leq k < q + 1 \Leftrightarrow \frac{q}{q+1} \leq \frac{R_{obsc}}{R} < \frac{q+1}{q+2} \quad (17)$$

Proof: From (14), we have

$$R = R_{obsc} + \lambda r_{obsc} \stackrel{(13)}{=} \beta r_{obsc} + \lambda r_{obsc} = (\beta + \lambda)r_{obsc}.$$

From Theorem 5, we know that

$$\begin{aligned} r_{min} &= \frac{Rr_{obsc}}{R - R_{obsc}} = \frac{(\lambda + \beta)r_{obsc}^2}{\lambda r_{obsc}} = \frac{\lambda + \beta}{\lambda} r_{obsc} \\ &= \frac{\lambda + k\lambda}{\lambda} r_{obsc} = (1 + k)r_{obsc}. \end{aligned}$$

This proves (15).

Now (3) and (15) yield:

$$\begin{aligned} r_{min} &= (1 + k)r_{obsc} = \frac{Rr_{obsc}}{R - R_{obsc}} \\ \Rightarrow k &= \frac{R}{R - R_{obsc}} - 1 = \frac{R_{obsc}}{R - R_{obsc}}. \end{aligned}$$

Hence, (16) is proven as well. Next, we prove (17). To this aim, we apply (16):

$$\begin{aligned} q \leq k &\stackrel{(16)}{=} \frac{R_{obsc}}{R - R_{obsc}} < q + 1 \\ \Leftrightarrow &\begin{cases} qR - qR_{obsc} \leq R_{obsc} \text{ and} \\ R_{obsc} < (q + 1)R - (q + 1)R_{obsc} \end{cases} \\ \Leftrightarrow &\begin{cases} R \leq \frac{q+1}{q}R_{obsc} \text{ and} \\ R > \frac{q+2}{q+1}R_{obsc} \end{cases} \\ \Leftrightarrow &\frac{q}{q+1} \leq \frac{R_{obsc}}{R} < \frac{q+1}{q+2} \end{aligned}$$

Therefore, (17) holds. \blacksquare

Corollary 2: Considering R fixed, a good choice for $\frac{R_{obsc}}{R}$ would be the middle of the interval $(\frac{q}{q+1}, \frac{q+1}{q+2})$. Therefore, we can choose

$$\frac{R_{obsc}}{R} = \frac{1}{2} \left(\frac{q}{q+1} + \frac{q+1}{q+2} \right)$$

In particular, for $q = 1$, we have:

$$1 \leq k < 2 \Leftrightarrow \frac{1}{2} \leq \frac{R_{obsc}}{R} < \frac{2}{3}$$

In this case, we can choose $R_{obsc} = \frac{7}{12}R$.

When $q \rightarrow \infty$, the ratio $\frac{R_{obsc}}{R} \rightarrow 1$ with a speed inversely proportional to q . Therefore, for large q , the location of obscurants tends to overlap with that of sensors.

Next, we derive an analytic formula for the size of the obscurant space expressed as a function of the object space size and the sizes of the individual obscurants.

Corollary 3: Using the assumptions in Theorem 6, we have:

$$R_{obsc,max} = \frac{1}{2} (2R + r_{obsc} - \sqrt{4Rr_{obsc} + r_{obsc}^2})$$

This expression for R_{obsc} is achieved for $\lambda = k$.

Proof: From (13) we derive:

$$R_{obsc} = k\lambda r_{obsc} \leq \frac{k^2 + \lambda^2}{2} r_{obsc} \quad (18)$$

In the above inequality, we have used the fact that $(k - \lambda)^2 \geq 0$. Equality, i.e. $(k - \lambda)^2 = 0$ is achieved iff $k = \lambda$. Therefore, by choosing $k = \lambda$, we obtain the maximal value for R_{obsc} :

$$R_{obsc,max} = k^2 r_{obsc}$$

From (16), we get:

$$\begin{aligned} R_{obsc,max} &= \frac{R_{obsc,max}^2}{(R - R_{obsc,max})^2} r_{obsc} \\ \Leftrightarrow R_{obsc,max}^2 - 2RR_{obsc,max} - r_{obsc}R_{obsc,max} + R^2 &= 0 \\ \Leftrightarrow R_{obsc,max}^2 - (2R + r_{obsc})R_{obsc,max} + R^2 &= 0 \end{aligned}$$

Solving for $R_{obsc,max}$ we get:

$$\begin{aligned} R_{obsc,max} &= \frac{1}{2} \left(2R + r_{obsc} \pm \sqrt{(2R + r_{obsc})^2 - 4R^2} \right) \\ &= \frac{1}{2} \left(2R + r_{obsc} \pm \sqrt{4Rr_{obsc} + r_{obsc}^2} \right) \end{aligned}$$

On the other hand, $R_{obsc,max}$ needs to satisfy (5). Using the expression of $R_{obsc,max}$ above in (5), we find that only the smaller of the roots satisfies, therefore:

$$R_{obsc,max} = \frac{1}{2} \left(2R + r_{obsc} - \sqrt{4Rr_{obsc} + r_{obsc}^2} \right)$$

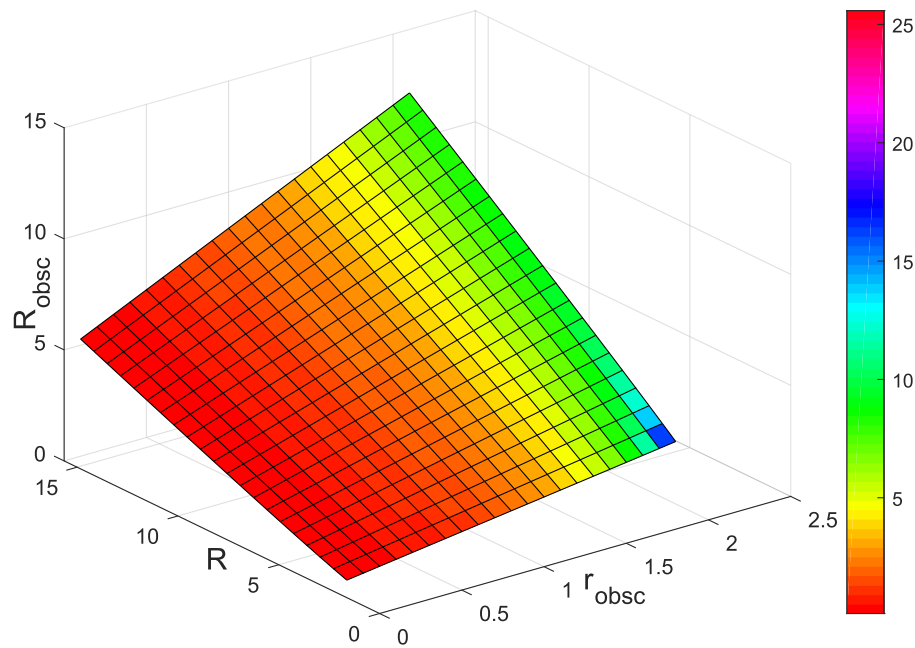
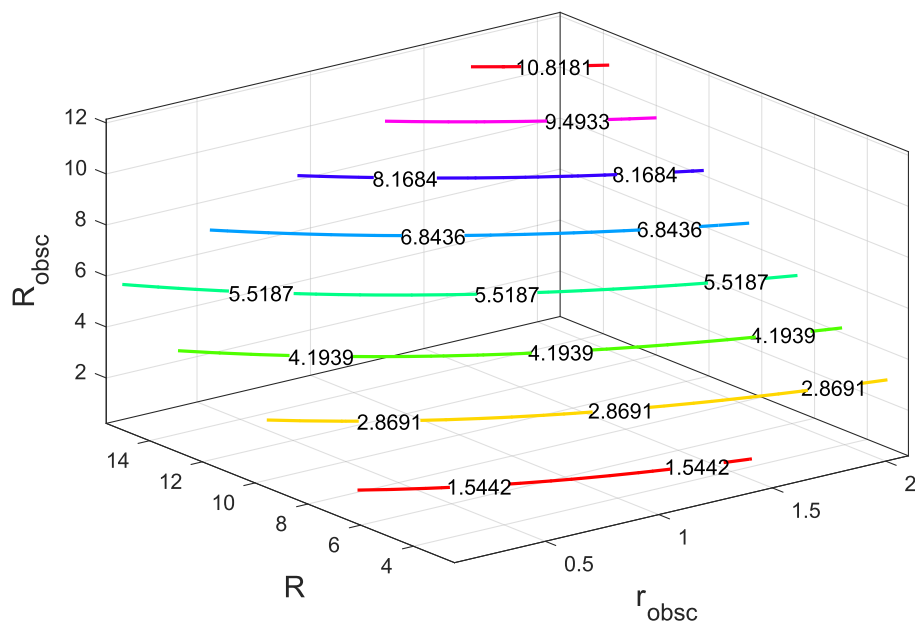
Corollary 3 provides an expression for the maximal value of the obscurant space. This result also shows that the radius of the obscurant space increases to infinity with the same speed as the radius of the sensor space. \blacksquare

IV. EXPERIMENTS

We discuss the relationships among r_{obsc} , R , R_{obsc} and r_{min} in two cases. In both cases, following the relations from Theorem 6, variables r_{obsc} and R are in a linear relationship. Variable R_{obsc} is chosen differently in each of the two cases as follows: 1) in the first case, the interval $(\frac{(r_{obsc}+R)-\sqrt{d}}{2}, \frac{(r_{obsc}+R)+\sqrt{d}}{2})$ is equally divided into several equally sized intervals and a value for R_{obsc} is selected in each small interval. 2) in the second case, R_{obsc} is set satisfying a linear relationship with R , i.e., r_{obsc} , R and R_{obsc} are in a linear relationship.

In the first case, the values of variables r_{obsc} , R and R_{obsc} are selected under the conditions in Theorem 5, i.e., $R > 6r_{obsc}$ and $R_{obsc} \in (\frac{(r_{obsc}+R)-\sqrt{d}}{2}, \frac{(r_{obsc}+R)+\sqrt{d}}{2})$. Moreover, there are 21 values of r_{obsc} ranging from 0.1 to 2.1. In order for R to satisfy the condition $R > 6r_{obsc}$, a ratio whose 21 values are $ratio = \{2.22, 2.82, \dots, 14.22\}$ with an equal difference of 0.6 is chosen. The values of R are obtained by $R = 1.1 * ratio$. As to the values of R_{obsc} , a variable called *step* is defined as follows: $step = \frac{\frac{(r_{obsc}+R)+\sqrt{d}}{2} - \frac{(r_{obsc}+R)-\sqrt{d}}{2}}{21} = \frac{\sqrt{d}}{21} = 0.3434$. Based on *step*, we set $R_{obsc} = \frac{(r_{obsc}+R)-\sqrt{d}}{2} + 0.01 + i * step$, where $i \in \{0, 1, \dots, 20\}$ and the value 0.01 is utilized to make the smallest R_{obsc} larger than $\frac{(r_{obsc}+R)-\sqrt{d}}{2}$.

In our experiments, we obtain the relationships among r_{obsc} , R_{obsc} , R and r_{min} by analyzing the figures. Firstly, a four dimension figure Fig. 3(a) is plotted with the values of r_{obsc} ,

(a) figure of r_{obscc} , R_{obscc} , R and r_{min} (colors in the figure denote values of r_{min})(b) contours of R_{obscc} Fig. 3. r_{obscc} and R are in a linear relationship, and they only limit the value range of R_{obscc} .

R_{obscc} , R independent of each other. In Fig. 3(a), r_{obscc} , R and R_{obscc} are drawn as x-axis, y-axis and z-axis, respectively. Moreover, the color in Fig. 3(a) represents the values of r_{min} . From Fig. 3(a), we derive the following observations: 1) the three-dimensional shape of the values of r_{obscc} , R and R_{obscc} form a lateral view of a tilted pyramid, which means the larger the values of both R and r_{obscc} , the larger the values of R_{obscc} ; 2) the value of r_{min} increases as the values of r_{obscc} , R and R_{obscc} increase. Moreover, the largest value of r_{min} is achieved when r_{obscc} is largest and both R and R_{obscc} are close to their smallest values. To observe the lateral view of the pyramid,

we drew its contours in Fig. 3(b). Any two adjacent contours are at an equal distance since the values of R_{obscc} are selected with the same *step*. Moreover, the contours are in an arc shape with different lengths.

Sub-figures in Fig. 4 are used to observe the hidden information in Fig. 3(a). In Fig. 4 (a), we make the following observation: the change in the values of r_{min} is relatively flat, until it exponentially approaches the maximum value of r_{min} . The same observation applies to Fig. 4 (b). In addition, Fig. 4 (b) shows how the value of R_{obscc} increases nonlinearly as the value of r_{obscc} increases.

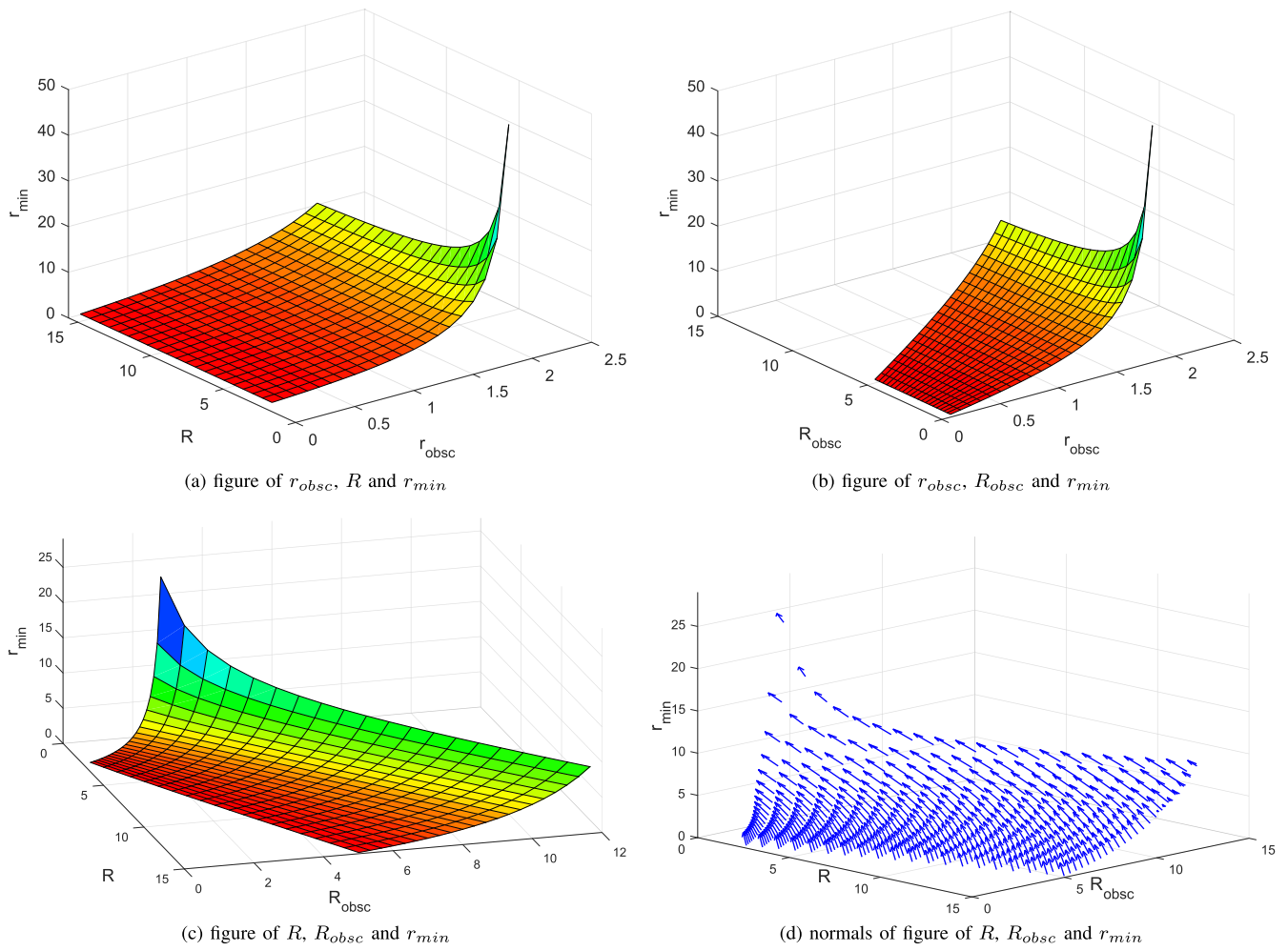


Fig. 4. Figures of r_{min} with two of r_{obs} , R_{obs} and R .

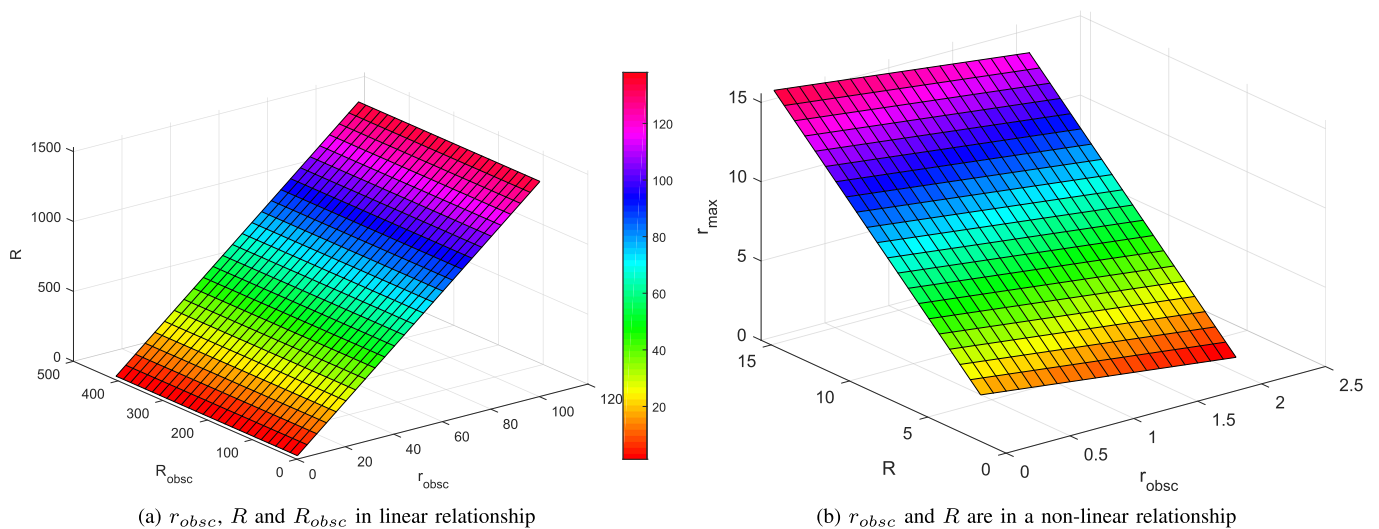


Fig. 5. (a) r_{min} , (b) r_{max} .

Based on Fig. 4 (c), we make the following observations: 1) when R approaches its smallest value in the figure, the value of r_{min} increases exponentially as the value of R_{obs} increases; 2) when R 's value approaches its largest value in the figure,

the value of r_{min} changes as the value of R_{obs} increases. The normals to the small polygonal faces in Fig. 4 (c) are drawn in Fig. 4 (d), represented by the arrows. From Fig. 4 (d), we draw the following observations: 1) when $R_{obs} < 5$ and

$R < 10$, the arrows are very close to each other. As both R_{obs} and R increase, the distances among arrows increase, showing that the value of r_{min} increases faster.

In the second case, we consider all three parameters r_{obs} , R and R_{obs} in a linear relationship with each other. From Fig. 5 (a), we observe that the value of r_{min} changes linearly as the values of the three parameters vary. Similarly to Fig. 4, we can draw three sub-figures from the data shown in Fig. 5 (a). We found that these are similar to Fig. 5 (a). Hence, we have omitted the sub-figures.

Fig. 5 (b) illustrates how the value of r_{max} changes as the values of R and r_{obs} change. They are in a simple linear relationship as stated in Theorem 6.

V. CONCLUSION

This paper presented an initial sensor modulator placement scenario and provided upper and lower bounds on the maximum number of signatures when the object space is large. We then extended our model with a detailed placement of sensors and obscurants. We built a mathematical model disclosing the relationship among the object space, the obscurant space, the detection space, and the sizes of individual obscurants. In this second scenario, we established the minimum and maximum size of the object space in which objects can be detected. We further expressed the size of the obscurant space as determined by the sensor space and the sizes of individual obscurants. Finally, we derived the maximum obscurant space size given the sensor space size and the sizes of the individual obscurants. These results provide insight into how to place obscurants relative to sensors and the center of the detection area to achieve a maximum area coverage. Intuitively, if obscurants are placed too close to sensors and too far from the objects to be detected, the whole object space can end up in the shadow of one or more obscurants, with few or no signatures being created. Conversely, obscurants should not be placed too far from sensors since this will reduce the size of the target object area where signatures are created. Our study provides concrete bounds for the target object area in terms of sensor and obscurant placement. We also quantify the distance at which obscurants should be placed between sensors and the object detection area and provide analytical formulas disclosing the relationship between obscurants, sensors, and the target area. These results can be used to avoid bad deployments and to provide guidance for binary sensors and obscurants placement in future deployments.

REFERENCES

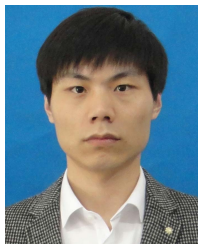
- [1] J. Atiga, M. Hamdi, R. Ejbali, and M. Zaided, "Recurrent neural network NARX for distributed fault detection in wireless sensor networks," *Int. J. Sens. Netw.*, vol. 37, no. 2, pp. 100–111, 2021.
- [2] D. J. Brady, N. P. Pitsianis, and X. Sun, "Reference structure tomography," *J. Opt. Soc. Amer. A, Opt., Image Sci., Vis.*, vol. 21, no. 7, pp. 1140–1147, 2004.
- [3] W. Zhou, F. Li, D. Li, X. Liu, and B. Li, "A human body positioning system with pyroelectric infrared sensor," *Int. J. Sensor Netw.*, vol. 21, no. 2, pp. 108–115, Jan. 2016.
- [4] S. Shioda, "Target counting with binary proximity sensors based on sensor-cluster identification," in *Proc. 11th Int. Conf. Mobile Ad Hoc Sensor Syst. (MASS)*, Oct. 2014, pp. 505–506.
- [5] L. Song and Y. Wang, "Multiple target counting and tracking using binary proximity sensors: Bounds, coloring, and filter," in *Proc. 15th ACM Int. Symp. Mobile Ad Hoc Netw. Comput.*, 2014, pp. 397–406.
- [6] T. Li *et al.*, *On Target Counting by Sequential Snapshots of Binary Proximity Sensors*, T. Abdelzaher, Ed. Berlin, Germany: Springer-Verlag, 2015, pp. 19–34.
- [7] L. Luo, Y. Xiao, and W. Liang, "Encoding space to count multi-targets with multiplexed binary infrared sensors," in *Proc. 15th Int. Conf. Mobile Ad-Hoc Sensor Netw. (MSN)*, Dec. 2019, pp. 390–394.
- [8] N. Kitbutrawat, H. Yamaguchi, and T. Higashino, "Localization of binary motion sensors in house," in *Proc. 13th Int. Wireless Commun. Mobile Comput. Conf. (IWCMC)*, Jun. 2017, pp. 1132–1137.
- [9] S. O. Al-Jazzar, S. A. Aldalameh, D. McLernon, and S. A. R. Zaidi, "Intruder localization and tracking using two pyroelectric infrared sensors," *IEEE Sensors J.*, vol. 20, no. 11, pp. 6075–6082, Jun. 2020.
- [10] Q. Hao, D. J. Brady, B. D. Guenther, J. B. Burchett, M. Shankar, and S. Feller, "Human tracking with wireless distributed pyroelectric sensors," *IEEE Sensors J.*, vol. 6, no. 6, pp. 1683–1696, Dec. 2006.
- [11] Q. Hao, F. Hu, and Y. Xiao, "Multiple human tracking and identification with wireless distributed pyroelectric sensor systems," *IEEE Syst. J.*, vol. 3, no. 4, pp. 428–439, Dec. 2009.
- [12] P. Rashidi, D. J. Cook, L. B. Holder, and M. Schmitter-Edgecombe, "Discovering activities to recognize and track in a smart environment," *IEEE Trans. Knowl. Data Eng.*, vol. 23, no. 4, pp. 527–539, Apr. 2011.
- [13] D. Yang and J. Huangfu, "Improving activity recognition for multiple-node wireless sensor network system based on compressed sensing," *Int. J. Sens. Netw.*, vol. 34, no. 3, pp. 162–171, 2020.
- [14] G. Liu, J. Liang, G. Lan, Q. Hao, and M. Chen, "Convolution neural network enhanced binary sensor network for human activity recognition," in *Proc. IEEE SENSORS*, Oct. 2016, pp. 1–3.
- [15] R. Ma, F. Hu, and Q. Hao, "Active compressive sensing via pyroelectric infrared sensor for human situation recognition," *IEEE Trans. Syst., Man, Cybern., Syst.*, vol. 47, no. 12, pp. 3340–3350, Dec. 2017.
- [16] X. Luo, Q. Guan, H. Tan, L. Gao, Z. Wang, and X. Y. Luo, "Simultaneous indoor tracking and activity recognition using pyroelectric infrared sensors," *Sensors*, vol. 17, no. 8, pp. 1701–1718, Apr. 2017.
- [17] B. Yang and Z. Meng, "Credit-based multiple human location for passive binary pyroelectric infrared sensor tracking system: Free from region partition and classifier," *IEEE Sensors J.*, vol. 16, no. 1, pp. 216–223, Jan. 2017.
- [18] J. Yan, P. Lou, R. Li, and J. Xiong, "Research on the multiple factors influencing human identification based on pyroelectric infrared sensors," *Sensors*, vol. 18, no. 2, pp. 1–22, Feb. 2018.
- [19] P. Yu, J. Yin, Y. Sun, Z. Du, and N. Cao, "An identity authentication method for ubiquitous electric power Internet of Things based on dynamic gesture recognition," *Int. J. Sens. Netw.*, vol. 35, no. 1, pp. 57–67, 2021.
- [20] P. Potluri, U. Gopinathan, J. R. Adleman, and D. J. Brady, "Lensless sensor system using a reference structure," *Opt. Exp.*, vol. 11, no. 8, pp. 965–974, Nov. 2003.
- [21] P. Potluri, M. Xu, and D. J. Brady, "Imaging with random 3D reference structures," *Opt. Exp.*, vol. 11, no. 18, pp. 2134–2141, Sep. 2003.
- [22] A. Sinha and D. J. Brady, "Size and shape recognition using measurement statistics and random 3D reference structures," *Opt. Exp.*, vol. 11, no. 20, pp. 2606–2618, Sep. 2003.
- [23] W. Sun, X. Zhang, X. Zhang, X. He, and G. Zhang, "Driving behaviour recognition based on orientation and position deviations," *Int. J. Sens. Netw.*, vol. 30, no. 3, pp. 161–171, 2019.
- [24] U. Gopinathan, D. J. Brady, and N. P. Pitsianis, "Coded apertures for efficient pyroelectric motion tracking," *Opt. Exp.*, vol. 11, no. 18, pp. 2142–2152, 2003.
- [25] A. H. Henni, R. Ben Bachouch, O. Bennis, and N. Ramdani, "Enhanced multiplex binary PIR localization using the transferable belief model," *IEEE Sensors J.*, vol. 19, no. 18, pp. 8146–8159, Sep. 2019.
- [26] Q. Guan, C. Li, L. Qin, and G. Wang, "Daily activity recognition using pyroelectric infrared sensors and reference structures," *IEEE Sensors J.*, vol. 19, no. 5, pp. 1645–1652, Mar. 2019.
- [27] L. Wu and Y. Wang, "Compressive sensing based indoor occupancy positioning using a single thermopile point detector with a coded binary mask," *IEEE Sensors Lett.*, vol. 3, no. 12, pp. 1–4, Dec. 2019.
- [28] N. Shrivastava, R. Mudumbai, U. Madhow, and S. Suri, "Target tracking with binary proximity sensors," *ACM Trans. Sensor Netw.*, vol. 2, no. 4, pp. 455–465, Nov. 2006.
- [29] P. K. Agarwal, D. Brady, and J. Matoušek, "Segmenting object space by geometric reference structures," *ACM Trans. Sensor Netw.*, vol. 2, no. 4, pp. 455–465, Nov. 2006.

- [30] P. Asadzadeh, L. Kulik, E. Tanin, and A. Wirth, "On optimal arrangement of binary sensors," in *Spatial Information Theory (Lecture Notes in Computer Science)*. Berlin, Germany: Springer-Verlag, Sep. 2011, pp. 168–187.
- [31] L. Luo, Y. Xiao, W. Liang, and M. Zheng, "A cell reconstruction tool to deploy binary pyroelectric sensor arrays," *IEEE Sensors J.*, vol. 20, no. 4, pp. 2117–2131, Feb. 2020.
- [32] L. Luo, Y. Xiao, and W. Liang, "The maximum number of cells with modulated binary sensors," *IEEE Sensors J.*, vol. 21, no. 9, pp. 11061–11074, May 2021.
- [33] M. Peng and Y. Xiao, "Signature maximization in designing wireless binary pyroelectric sensors," in *Proc. IEEE Global Telecommun. Conf.*, Dec. 2010, pp. 1–5.
- [34] M. Peng, Y. Xiao, N. Li, and X. Liang, "Monitoring space segmentation in deploying sensor arrays," *IEEE Sensors J.*, vol. 14, no. 1, pp. 197–209, Jan. 2014.
- [35] Accessed: Jan. 2022. [Online]. Available: https://en.wikipedia.org/wiki/Intercept_theorem
- [36] Accessed: Jan. 2022. [Online]. Available: https://en.wikipedia.org/wiki/Tangent_lines_to_circles



Alina Olteanu (Member, IEEE) received the B.S. degree in computer science from the University of Bucharest and the M.S. degree in applied mathematics from the Polytechnic University of Bucharest, Romania, and the M.S. and Ph.D. degrees in computer science from The University of Alabama in 2007 and 2009, respectively. Prior to joining the University of Montevallo, Dr. Olteanu worked as a Software Consultant/a Developer of building enterprise applications for the banking and healthcare industries. She is

currently an Assistant Professor in computer science with the University of Montevallo. She is also working as the Coordinator of the Computer Science Program at UM. She was responsible for launching the program in 2019. Her current research interests are in wireless networks, network security, and network optimization. She has devoted her research activities to modeling various problems in wireless and sensor network security. In computer science education, she is passionate about curriculum development and promoting an interactive learning environment.



Longxiang Luo (Member, IEEE) received the B.E. degree from Gaungxi University, China, in 2012, and the Ph.D. degree from the Shenyang Institute of Automation, Chinese Academy of Sciences, China, in 2021. He is currently a Postdoctoral Researcher with the Laboratory of Neural Mechanism, Motor Control Institute of Neuroscience, Chinese Academy of Sciences, Shanghai, China. His research interests include space segmentation, sensing optimization, brain–computer interface (BMI), motion control, and planning of robotic arms.



Yang Xiao (Fellow, IEEE) received the B.S. and M.S. degrees in computational mathematics from Jilin University, Changchun, China, in 1989 and 1991, respectively, and the M.S. and Ph.D. degrees in computer science and engineering from Wright State University, Dayton, OH, USA, in 2000 and 2001, respectively.

He is currently a Full Professor with the Department of Computer Science, The University of Alabama, Tuscaloosa, AL, USA.

He had directed 20 doctoral dissertations and supervised 19 M.S. theses/projects. He has published over 300 science citation index (SCI)-indexed journal articles (including over 60 IEEE/ACM TRANSACTIONS) and 300 engineering index (EI)-indexed refereed conference papers and book chapters related to these research areas. His current research interests include cyber-physical systems, the Internet of Things, security, wireless networks, smart grid, and telemedicine. Prof. Xiao was a Voting Member of the IEEE 802.11 Working Group from 2001 to 2004, involving the IEEE 802.11 (Wi-Fi) standardization work. He is an IET Fellow and an AAIA Fellow. He has served as a Guest Editor over 30 times for different international journals, including the IEEE JOURNAL ON SELECTED AREAS IN COMMUNICATIONS in 2022, IEEE TRANSACTIONS ON NETWORK SCIENCE AND ENGINEERING in 2021, IEEE TRANSACTIONS ON GREEN COMMUNICATIONS AND NETWORKING in 2021, IEEE NETWORK in 2007, IEEE WIRELESS COMMUNICATIONS in 2006 and 2021, *IEEE Communications Standards Magazine* in 2021, and *Mobile Networks and Applications (MONET)* (ACM/Springer) in 2008. He also serves as the Editor-in-Chief for *Cyber-Physical Systems* journal, *International Journal of Sensor Networks (IJSNet)*, and *International Journal of Security and Networks (IJSN)*. He has been serving as an Editorial Board Member or an Associate Editor for 20 international journals, including the IEEE TRANSACTIONS ON NETWORK SCIENCE AND ENGINEERING (TNSE) since 2022, IEEE TRANSACTIONS ON CYBERNETICS since 2020, IEEE TRANSACTIONS ON SYSTEMS, MAN, AND CYBERNETICS: SYSTEMS from 2014 to 2015, IEEE TRANSACTIONS ON VEHICULAR TECHNOLOGY from 2007 to 2009, and IEEE COMMUNICATIONS SURVEYS AND TUTORIALS from 2007 to 2014.



Wei Liang (Senior Member, IEEE) received the Ph.D. degree in mechatronic engineering from the Shenyang Institute of Automation, Chinese Academy of Sciences, Shenyang, China, in 2002. She is currently a Full Professor with the Shenyang Institute of Automation, Chinese Academy of Sciences. As a Primary Participant/a Project Leader, she developed the WIA-PA and WIA-FA standards for industrial wireless networks, which are specified by IEC 62601 and IEC 62948, respectively. Her research

interests include industrial wireless sensor networks and wireless body area networks. Dr. Liang received the International Electrotechnical Commission 1906 Award in 2015 as a Distinguished Expert of industrial wireless network technology and standard.